Australian Government
Department of Defence
Defence Science and
Technology Organisation

Landmark-based Navigation of an Unmanned Ground Vehicle (UGV)

Jijoong Kim and Hatem Hmam

Weapons Systems Division
Defence Science and Technology Organisation

DSTO-TR-2260

ABSTRACT

We present a method for estimating the position and orientation of a ground vehicle in an environment with landmarks. From the geometric relationships, we derive a set of linear equations with a quadratic constraint, which forms the basis for our optimisation problem. We also extend the problem to associating two sets of measurements taken at two successive locations to improve the navigation accuracy. This method is efficient and the performance is robust against large measurement errors.

Published by

Weapons Systems Division
DSTO Defence Science and Technology Organisation
PO Box 1500
Edinburgh South Australia 5111 Australia

Telephone: (08) 8259 5555
Fax: (08) 8259 6567

AR-014-415
March 2009

APPROVED FOR PUBLIC RELEASE

Landmark-based Navigation of an Unmanned Ground Vehicle (UGV)

Executive Summary

We present an efficient method for localising an unmanned ground vehicle (UGV) in a two dimensional environment with landmarks. We assume that the vehicle can identify these landmarks and measure their bearings. We derive a set of linear equations that relate the UGV's position and orientation to the measured bearings, assuming perfect measurements. Having noise in the measurements, we establish an estimator, based on minimising a constrained quadratic cost function.

Landmark-based navigation is useful where GPS is not adequate because of signal blockage and interference. Possible defence applications include robots performing the following tasks: indoor bomb search, landmine location, autonomous surveillance of military bases or nuclear sites, and logistics in urban battle zones.

The proposed algorithm is efficient and the performance is consistent given that the UGV is inside the boundary formed by the landmarks. The estimation accuracy is shown to improve as the number of landmarks increases. Given that the number of landmarks is limited, we extend the initial formulation and propose another method that utilises two sets of measurements from two locations and estimates the current position and azimuth with significantly improved accuracy. The performance is robust against large measurement errors, and can be coupled with an inertial navigation system to enable higher rate navigation with greater accuracy, especially in outdoor settings.

Authors

Jijoong Kim
Weapons Systems Division

Jijoong Kim received a B.E. (Hons) in Electrical and Electronic Engineering and M.EngSc. both from the University of Adelaide in 1993 and 1995 respectively. He was a research assistant at the EE department of the University of Adelaide for six months, and then joined DSTO in November 1995. During his employment with DSTO, he completed a PhD in Image Processing and Computer Vision from the University of Wollongong in 2006. Since 1995, he has been with the Guidance and Control Group. His research interests include: Missile Guidance, Optimal Control, Navigation, and Computer Vision.

Hatem Hmam
Electronic Warfare and Radar Division

Hatem Hmam received his Ph.D. degree in Electrical Engineering from University of Cincinnati, Ohio, USA, in 1992. He then pursued post-doctoral research in jet engine control at University of Colorado, Boulder, and signal processing at Queensland University of Technology, Brisbane. He joined DSTO in 1996 and worked in WSD and EWRD Divisions. He is currently a member of Distributed Electronic Warfare group where he is developing and implementing passive localisation techniques of RF emitters.

Contents

Acronyms

CRLB	**Cramer Rao Lower Bound**
GED	**Generalised Eigen-Decomposition**
GPS	**Global Positioning System**
INS	**Inertial Navigation System**
MLE	**Maximum Likelihood Estimator**
RMS	**Root Mean Square**
SVD	**Singular Vector Decomposition**
TMA	**Two Measurements Association**
UAV	**Unmanned Aerial Vehicle**
UGV	**Unmanned Ground Vehicle**

1. Introduction

This report presents the problem of estimating the position and azimuth of a mobile robot or unmanned ground vehicle (UGV), by measuring bearing angles to landmarks. We derive a set of linear homogenous equations that relate the robot position and orientation to the measured bearings. Given that bearing measurements are noisy and redundant, we establish an estimator based on minimising a constrained quadratic cost function.

Localisation is of interest for many industrial (e.g., robots) and defence applications (e.g., UAVs and UGVs). In open outdoor environments, differential GPS systems can provide precise position information. However, there are scenarios where GPS is not adequate such as indoor, underwater, extraterrestrial or urban environments, because of signal blockage and multipath interference. Also, for stand-alone systems, the position accuracy may not be sufficient [Borenstein et al, 1997]. In defence applications, the GPS receiver on the ground level is likely to be subject to jamming or spoofing from an adversary. A simple alternative would be odometry or inertial navigation system (INS). However, both of which are subject to build-up of error with time, and often require an external aid.

Landmark based localisation is attractive in a controlled environment where the landmarks can be precisely located. Possible applications include robots performing one or more of the following tasks: indoor bomb search, landmine location, autonomous surveillance of military bases or nuclear sites, and logistics in urban battle zones.

We assume that the robot is equipped with an omni-directional camera (e.g., catadioptric sensor, ringcam, panospheric camera) [Daniilidis, K, web source].

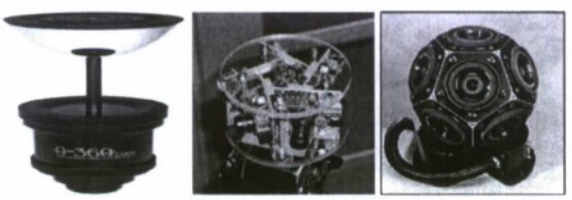

Figure 1: Examples of omni-directional cameras [Daniilidis, K, web source]

The report is organised as follows. In Section 2, we present the formulation of the basic algorithm and optimisation, and performance assessment. In Section 3, we extend the problem by taking two sets of measurements at two successive locations and combining them to improve the localisation accuracy. Section 4 summarises the findings and concludes the report.

2. Formulation of Basic Algorithm

2.1 Notations

X^A: vector X in frame A - (note that without A, default frame is REF which is a fixed reference frame).

$\mathbf{L}_i = \begin{bmatrix} X_{Li} \\ Y_{Li} \end{bmatrix}$: i[th] landmark position vector

$\mathbf{B}_1 = \begin{bmatrix} X_{Bi} \\ Y_{Bi} \end{bmatrix} = \mathbf{B}_1^R$: robot position at i[th] time instance.

$\mathbf{R}_A^B$: 2x2 rotation matrix for coordinate transformation from frame A to frame B.

Rotation Matrices (and shorthand notations):

$$\mathbf{R}_R^{B1} = \begin{bmatrix} \cos\theta_1 & \sin\theta_1 \\ -\sin\theta_1 & \cos\theta_1 \end{bmatrix} = \begin{bmatrix} c_1 & s_1 \\ -s_1 & c_1 \end{bmatrix} \text{ REF to Robot at Position 1}$$

$$\mathbf{R}_R^{B2} = \begin{bmatrix} \cos\theta_2 & \sin\theta_2 \\ -\sin\theta_2 & \cos\theta_2 \end{bmatrix} = \begin{bmatrix} c_2 & s_2 \\ -s_2 & c_2 \end{bmatrix} \text{ REF to Robot at Position 2}$$

$$\mathbf{R}_{B2}^{B1} = \begin{bmatrix} \cos(\Delta\theta) & \sin(\Delta\theta) \\ -\sin(\Delta\theta) & \cos(\Delta\theta) \end{bmatrix} = \begin{bmatrix} c & s \\ -s & c \end{bmatrix} \text{ Robot 2 to Robot 1}$$

Note all the angular terms are positive when measured counter-clockwise.

Given a robot positioned at **B1**, consider an i[th] landmark position $\mathbf{L}_i$ expressed in body frame (see Figure 2),

$$\mathbf{L}_i^{B1} = \begin{bmatrix} L_{1i}\cos\beta_{1i} \\ L_{1i}\sin\beta_{1i} \end{bmatrix} = \mathbf{R}_R^{B1}(\mathbf{L}_i - \mathbf{B}_1) = \mathbf{R}_R^{B1}\mathbf{L}_i - \mathbf{R}_R^{B1}\mathbf{B}_1 = \begin{bmatrix} \cos\theta_1 & \sin\theta_1 \\ -\sin\theta_1 & \cos\theta_1 \end{bmatrix} \begin{bmatrix} X_{Li} \\ Y_{Li} \end{bmatrix} + \mathbf{T}_1^{B1} \quad (1)$$

where $\mathbf{T}_1^{B1} = \begin{bmatrix} X_T \\ Y_T \end{bmatrix} = -\mathbf{R}_R^{B1}\mathbf{B}_1$. (2)

2.2 Derivation of Linear Equations

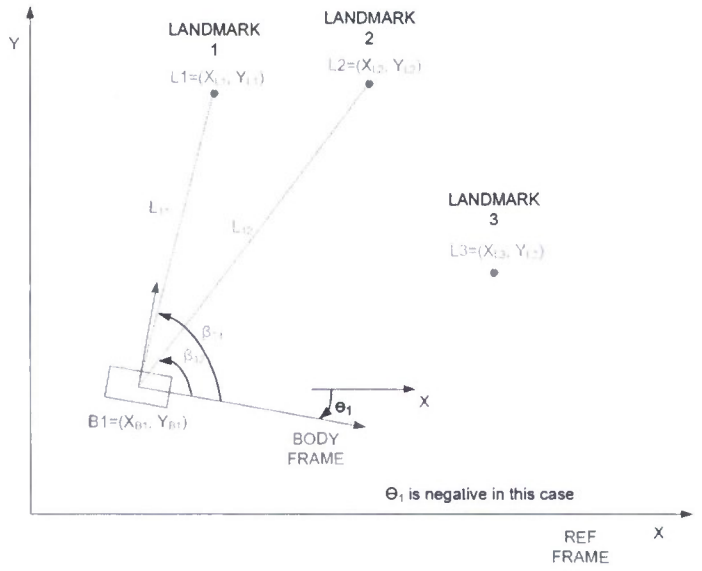

*Figure 2: Illustration of a mobile robot that detects three known landmarks along the directions $\beta_{11},\beta_{12},\beta_{13}$. The problem is to find the position **B1** and orientation θ_1 of the robot with respect to REF frame.*

Dividing the top row by bottom row gives

$$\frac{\cos\beta_{1i}}{\sin\beta_{1i}} = \frac{\cos\theta_1 X_{Li} + \sin\theta_1 Y_{Li} + X_T}{-\sin\theta_1 X_{Li} + \cos\theta_1 Y_{Li} + Y_T}.$$

This can be rewritten in vector form as

$$\left[\sin\beta_{1i}X_{Li} - \cos\beta_{1i}Y_{Li},\quad \sin\beta_{1i}Y_{Li} + \cos\beta_{1i}X_{Li},\quad \sin\beta_{1i},\quad -\cos\beta_{1i}\right]\cdot\begin{bmatrix}\cos\theta_1\\ \sin\theta_1\\ X_T\\ Y_T\end{bmatrix} = 0 \qquad (3)$$

Let

$A11_i = \sin\beta_{1i}X_{Li} - \cos\beta_{1i}Y_{Li}$

$A12_i = \sin\beta_{1i}Y_{Li} + \cos\beta_{1i}X_{Li}$.

In the absence of measurement errors, populating (3) for all N landmarks will produce N homogenous equations which can be expressed as a vector equation

$$\begin{bmatrix} Al1_1 & Al2_1 & \sin\beta_{11} & -\cos\beta_{11} \\ Al1_2 & Al2_2 & \sin\beta_{12} & -\cos\beta_{12} \\ \mathrm{M} & \mathrm{M} & \mathrm{M} & \mathrm{M} \\ Al1_N & Al2_N & \sin\beta_{1N} & -\cos\beta_{1N} \end{bmatrix} \cdot \begin{bmatrix} \cos\theta_1 \\ \sin\theta_1 \\ X_T \\ Y_T \end{bmatrix} = \mathbf{0}_{N\times 1} \tag{4}$$

We express the above equation as $\mathbf{Ax} = \mathbf{b}$ where $\mathbf{A}$ is the measurement matrix, $\mathbf{x}$ contains the three unknowns we want to estimate (ie,. θ_1, X_T, Y_T), and $\mathbf{b} = \mathbf{0}_{N\times 1}$. If the bearing measurements and landmark positions are error free, then the exact solution to (4) can be found with N=3, as long as the landmarks and the robot do not lie on a circle or a straight line [Shimshoni, I., 2002]. If the measurements are noisy and more landmarks are available, then we need to establish a cost function and minimise it to solve the localisation problem.

2.3 Optimal Solution

Note that the matrix $\mathbf{A}$ contains the bearing measurements. If the measurements are noisy, then $\mathbf{b}$ will no longer be equal to $\mathbf{0}_{n\times 1}$. The objective is to minimise the cost function defined as $(\mathbf{Ax})^T\mathbf{Ax}$ which would typically be non-zero.

We want to minimise

$$\mathbf{x}^T\mathbf{Px} \tag{5}$$

subject to

$$\mathbf{x}^T\mathbf{Qx} - 1 = 0 .$$

where $\mathbf{P} = \mathbf{A}^T\mathbf{A}$, and $\mathbf{Q} = \begin{bmatrix} 1 & 0 & 0 & 0 \\ 0 & 1 & 0 & 0 \\ 0 & 0 & 0 & 0 \\ 0 & 0 & 0 & 0 \end{bmatrix}$.

The constraint $\mathbf{x}^T\mathbf{Qx} - 1 = 0$ expresses the known property, $\cos^2\theta_1 + \sin^2\theta_1 = 1$.

Now define the Lagrangian of (5) as

$$L(\mathbf{x}, \lambda) = \mathbf{x}^T\mathbf{Px} - \lambda(\mathbf{x}^T\mathbf{Qx} - 1) \tag{6}$$

The minimiser of Equation 6 must satisfy the first optimality condition (7) and the constraint (8) shown below

$$\frac{\partial L}{\partial \mathbf{x}} = 2(\mathbf{P} - \lambda\mathbf{Q})\mathbf{x} = 0 \tag{7}$$

$$\frac{\partial L}{\partial \lambda} = \mathbf{x}^T\mathbf{Qx} - 1 = 0 . \tag{8}$$

Solving (7) and (8) becomes a generalised eigen-decomposition (GED) problem. The optimal Lagrange multiplier λ^* is the smallest positive eigenvalue of the matrix pair $(\mathbf{P},\mathbf{Q})$ and $\mathbf{x}^*$ is the corresponding eigenvector, normalised according to (8).

2.4 Implementation Issues

This formulation bears resemblance to the method proposed by [Shimshoni, 2002]. Shimshoni applies a number of pre-conditioning processes to the linear equations to arrive at the same equation as in (4). The main difference is that the constraints used by Shimshoni is $\mathbf{x}^T\mathbf{x}=1$ instead of $\mathbf{x}^T\mathbf{Q}\mathbf{x}-1=0$, and therefore SVD is employed to solve the localisation problem.

It should be noted that for numerical stability, it is often necessary to translate and scale the original geometry so that the entries of $\mathbf{A}$ are numerically comparable in size.

First, we shift the origin of the REF frame to a mean of all the landmark positions, and then replace $\mathbf{L}_i$ with $\acute{\mathbf{L}}_i$ where $\acute{\mathbf{L}}_i=\mathbf{L}_i-\frac{1}{N}\sum_i^N\mathbf{L}_i$ (N is the number of landmarks). We then compute the norms $\|\acute{\mathbf{L}}_i\|$ (ie, distance of each landmark from the new origin), find the maximum norm (named *SF*), and divide $\acute{\mathbf{L}}_i$ by *SF*. This process limits the position terms within ± 1, hence making them comparable to the magnitude of sine and cosine terms in (3).

When the optimal solution is found, we need to convert $\mathbf{T}_1^{B1}(=\mathbf{x}^*(3:4))$ to $\mathbf{B}_1$ (ie., robot position in REF frame) via following transformation.

$$\mathbf{B}_1=-SF*\left(\mathbf{R}_R^{B1}\right)^T\mathbf{T}_1^{B1}+\frac{1}{N}\sum_i^N\mathbf{L}_i \tag{9}$$

When the SVD or GED problem is solved, the solution is a unit eigenvector whose magnitude and sign need to be adjusted. First we have to satisfy $\mathbf{x}(1)^2+\mathbf{x}(2)^2=1$, by dividing $\mathbf{x}^*$ by $norm(\mathbf{x}^*(1:2))$. To resolve the sign issue, we perform the following routine.

***** Algorithm ********

1. compute the robot azimuth (θ_1) and position ($\mathbf{B}_1$) from $\mathbf{x}^*$.
2. given $\mathbf{L}_i$, $\mathbf{B}_1$ and θ_1, the expected bearing β_{1i} is computed.
3. For all landmarks, compare the computed bearings with the measured bearings. If the majority of the "computed-measured" bearing pairs are well aligned, then accept the solution. If the majority of them are off by about $180°$, then change the sign of $\mathbf{x}^*$ and recompute (9).

2.5 Performance Comparisons with Shimshoni's Method

We reproduced the work of Shimshoni to use as a benchmark. Here we show that our GED-based optimisation performs consistently better than the benchmark, and exclude SVD method in the performance comparison in Section 3.5.

We tested both methods, using two sets of 4 and 8 landmarks located at

L={(0, 0), (40, 0), (0, 40), (40, 40)} and
L={(0, 0), (40, 0), (0, 40), (40, 40), (20, 0), (0, 20), (40, 20), (20, 40)}.

We conducted 1000 Monte-Carlo simulations to get the statistics for the estimation errors. Note the robot azimuth is set to be uniformly distributed between -180° and180°. The bearing error is assumed to be Gaussian with standard deviations of 3° by default. Robot position is fixed at (4, 10).

2.5.1 Effects of Number of Landmarks

Using 4 landmarks, bearing std=3°

As shown in Figure 3, both methods generate error distribution Gaussian-like histograms of zero mean.

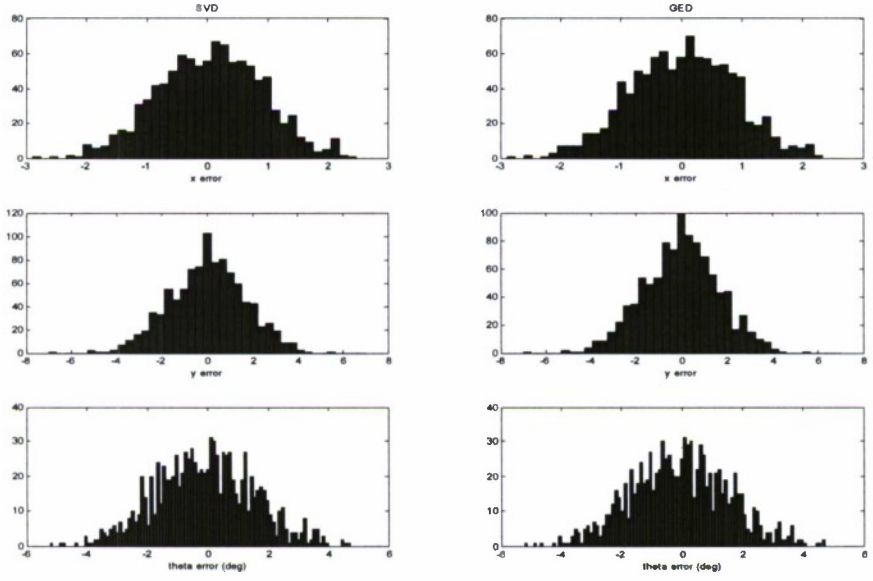

Figure 3: Histogram of x, y position and azimuth errors (from top to bottom) using SVD (left) and GED (right) optimisations, with bearing error standard deviation of 3°. Four landmarks are used.

The comparisons of the estimation errors between the SVD and GED methods are given as RMS (root mean square) values in Table 1. The GED method produces smaller errors but the difference is not significant.

Table 1: Estimation errors (rms) obtained using both methods with four landmarks. The smaller numbers are shaded with pale yellow.

RMS error	SVD	GED
X position Error	0.8452	0.8444
Y position Error	1.5839	1.5780
Azimuth Error (°)	1.6239	1.6218

Using 8 landmarks, bearing std=3°

When the bearing measurements are increased to 8, the error distribution curves become more peaked (see Figure 4). Again, the performance difference is very small.

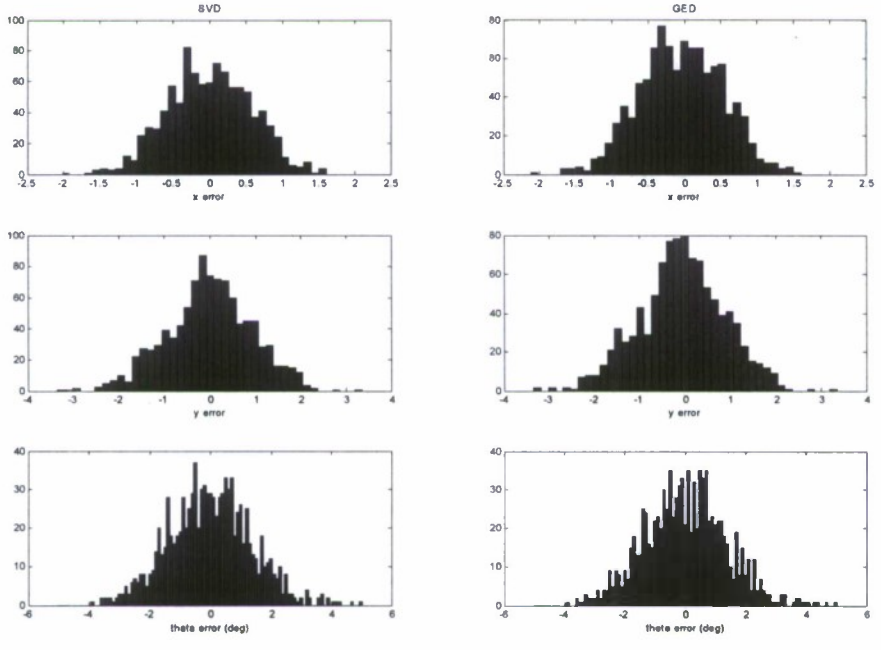

Figure 4: Histogram of x, y positions and azimuth errors (from top to bottom) using SVD (left) and GED (right) optimisations, with bearing error standard deviation of 3°. 8 landmarks are used.

Table 2: Estimation errors (rms) when eight landmarks are used

RMS error	SVD	GED
X position Error	0.5832	0.5822
Y position Error	0.9037	0.8969
Azimuth Error (°)	1.3764	1.3744

It is clear that the estimation accuracy of both methods improve when more measurements are available.

2.5.2 Effect of Measurement Noise

Here, we set N=4, and vary the bearing measurement error (1σ) from 1° to 10°. We introduce the Cramer-Rao Lower Bound (CRLB) which is the smallest possible error bound that any unbiased method could achieve for the same N, $\sigma(\beta)$ and robot-landmark geometry. We present the error curves for the GED/SVD along with the CRLB (see Figure 5) to show how close they are to the CRLB for various $\sigma(\beta)$ values. In Figure 5, the gaps among the three curves are small for $\sigma(\beta)$ up to 5°. As the bearing error becomes larger the gaps with the CRLB become wider. The GED method appears to outperform the SVD method even though the differences remain small.

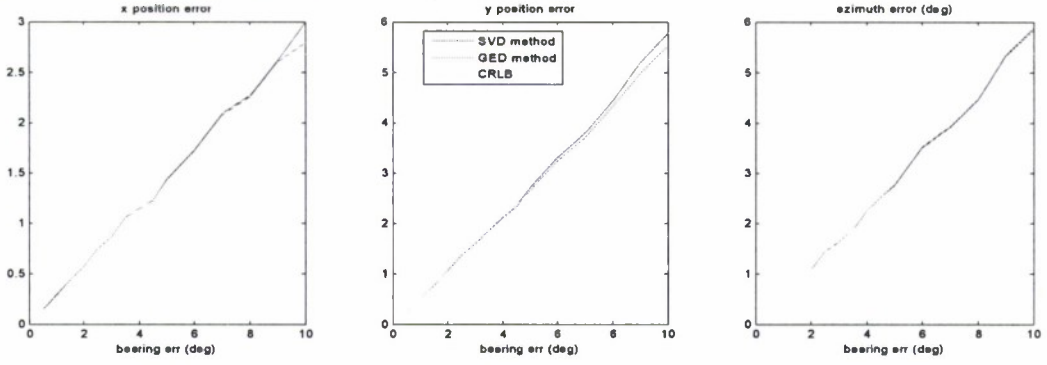

Figure 5: Plots of position and azimuth errors versus bearing errors (1σ). The red and blue curves represent the rms errors from the SVD and GED methods respectively. The green curves represent the Cramer-Rao Lower Bounds.

Figure 6 shows the estimation error differences between the SVD and GED methods. The values are mostly positive indicating that the GED method outperforms consistently. The error separation widens as the $\sigma(\beta)$ increases, indicating the GED method is more resilient against measurement noise.

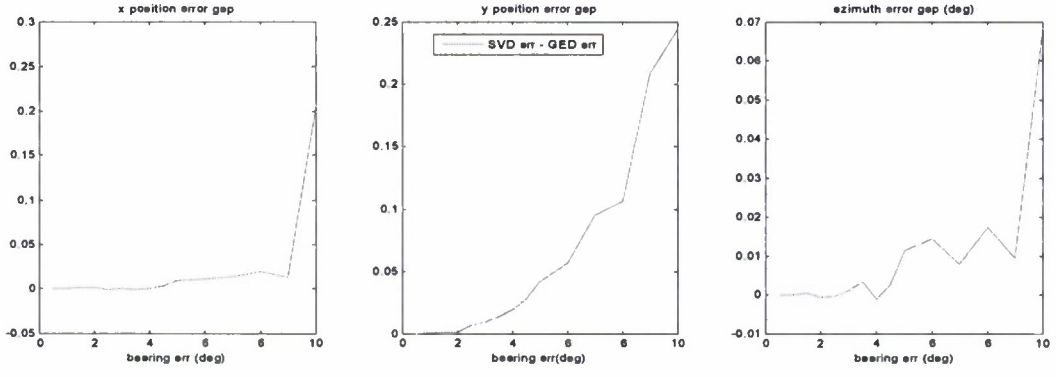

Figure 6: Estimation error differences between the SVD and GED estimation methods as functions of bearing error. A positive value means the error from the SVD method is larger than the error from the GED method.

2.5.3 Effect of Landmarks and Robot Geometry

The findings in Sections 2.5.1 and 2.5.2 are based on the fixed robot position of (4, 10). If the estimation accuracy varies drastically as the robot position varies, then the validity of the previous results may not hold.

In this subsection, we place the robot at 13 different locations and examine how the geometry affects the performance. In Figure 7, four landmarks are placed on the corners of a square (in green), and the robot positions are varied from the middle of the square to well outside the square. The combined position errors ($\sqrt{x\_err^2 + y\_err^2}$) and azimuth errors achieved from those positions are presented in Table 3. The second row shows the coordinates of the 13 locations, and the 1σ estimation errors are in the 3rd and 4th rows.

It is observed that the errors are small when the robot is within the square region (yellow shade in Table 3). Moving away from the centre does not cause noticeable increase in the estimation errors as long as the robot is kept within the perimeter. As the robot reaches the perimeter, the error increase becomes somewhat more evident (grey shade). Once outside the perimeter, then the errors become large and they increase rapidly as the robot moves further away from the landmarks. The optimisation seems to work best if bearings are widely scattered. As the robot moves further away from the square, the bearings aggregate in one direction. This kind of geometric arrangement (eg., position 13) seems to flatten the cost curve, making the minimum prone to the measurement noise. Of course, this spread can be reduced if the measurement noise is reduced making the cost curve smoother.

Another interesting observation is the large jump in the error at positions 8 and 9. This is the case when the landmarks and robot form a circle accidentally. In this case, an infinite number of solutions exist. The robot can be anywhere on the circle (shown in cyan) and receive the same bearing measurements [Betke, M., and Gurvits, L., 1997].

In summary, localisation is most accurate when the robot operates within the boundary formed by the landmarks.

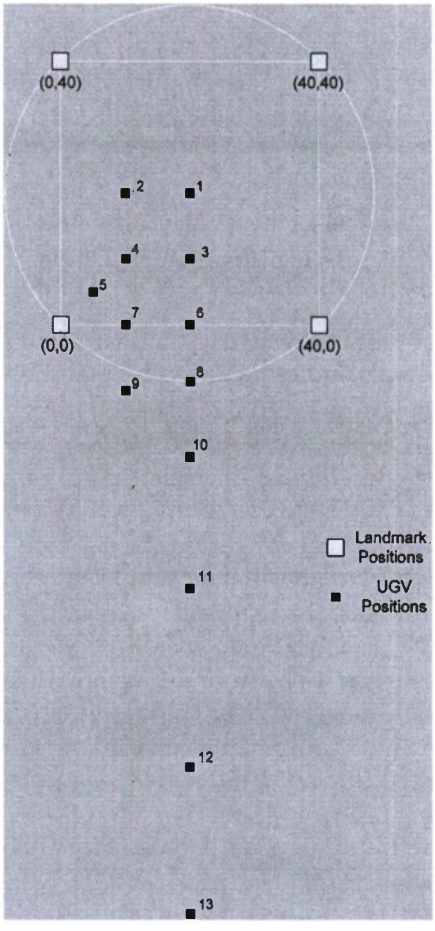

Figure 7: With four landmarks forming a square, 13 different robot positions are selected to examine the effect of the robot position on the estimation accuracy

Table 3: The position and azimuth errors achieved at 13 different robot locations

index	1	2	3	4	5	6	7	8	9	10	11	12	13
coords	20, 20	10, 20	20, 10	10, 10	5, 5	20, 0	10, 0	20,-8.3	10, -10	20, -20	20, -40	20, -70	20,-100
d Err	1.45	1.54	1.57	1.54	1.68	2.81	2.83	39.7	9.83	5.43	7.47	15.57	26.49
az Err	1.51	1.47	1.46	1.51	1.65	2.11	2.39	51.38	11.99	6.10	5.84	7.67	9.53

2.6 Nonlinear Least Square Estimation - Fine Tuning

The accuracy of the above estimation can be improved by considering an alternative objective function that directly compares the computed bearings to the measured bearings. For a given robot position and orientation, the bearing angle to the i[th] landmark is derived as

$$\beta_i = f_i(\mathbf{x}) = \tan^{-1}\left(\frac{\cos\theta(X_{Li} - X_B) + \sin\theta(Y_{Li} - Y_B)}{-\sin\theta(X_{Li} - X_B) + \cos\theta(Y_{Li} - Y_B)}\right) \tag{10}$$

where $\mathbf{x} = [\theta, X_B, Y_B]^T$ and $i = 1\text{K}\ N$. Note that this function is non-linear.
In practice the measured bearing is contaminated with additive noise as

$$\hat{\beta}_i = f_i(\mathbf{x}) + n_i \tag{11}$$

With N measurement, we stack up all bearing measurements to form a $N \times 1$ measurement vector

$$\hat{\boldsymbol{\beta}} = \mathbf{f}(\mathbf{x}) + \mathbf{n} \tag{12}$$

The problem objective is to find $\mathbf{x}$ that minimises the non-linear cost function

$$\mathbf{Q}(\mathbf{x}) = \left[\hat{\boldsymbol{\beta}} - \mathbf{f}(\mathbf{x})\right]^T \mathbf{N}^{-1}\left[\hat{\boldsymbol{\beta}} - \mathbf{f}(\mathbf{x})\right] \tag{13}$$

where

$\mathbf{N} = E[(\mathbf{n} - E[\mathbf{n}])(\mathbf{n} - E[\mathbf{n}])^T]$ is the measurement error covariance matrix. (14)

Note that if the bearing noise, $\mathbf{n}$, is Gaussian, then the above estimator becomes the *Maximum Likelihood Estimator* (MLE). In order to utilise the MLE, the estimate from the SVD/GED method is set as the initial estimate $\hat{\mathbf{x}}_0$ for the MLE, and a new $\hat{\mathbf{x}}$ is found via a gradient descent approach. The detailed formulation is given in Appendix B. Figure 8 shows further reduction of the estimation error using the MLE - the red curves are brought closer to the green curves.

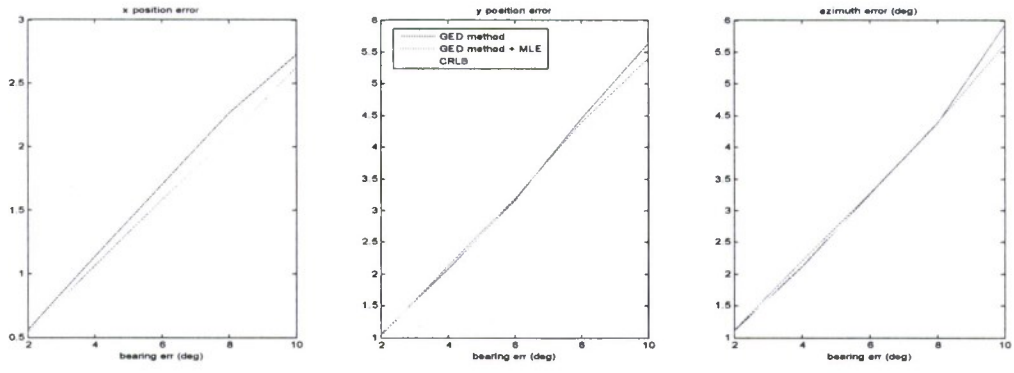

Figure 8: The estimation errors from GED method (blue), GED method followed by MLE (green), and CRLB(red) obtained using 4 measurements

We repeated the test using 8 landmarks to see the extent of the improvement. In Figure 9, the red curves are now much closer to the green curves (CRLB) than in Figure 8.

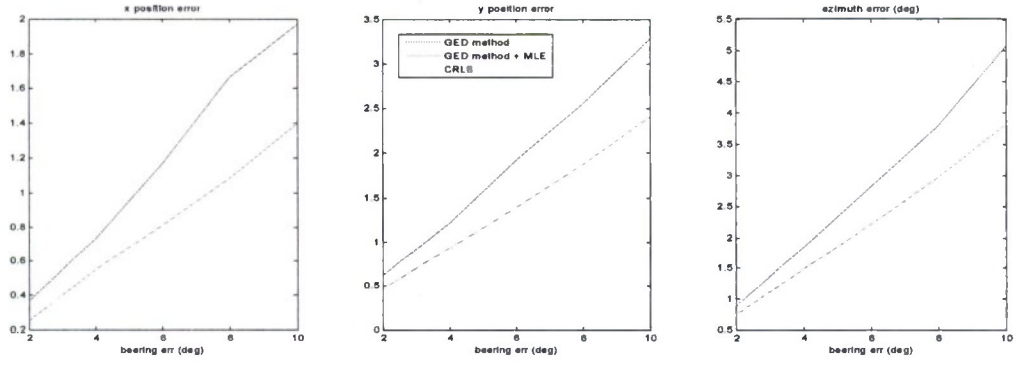

Figure 9: The estimation errors of GED method (blue), GED method followed by MLE (green), and CRLB(red) when 8 landmarks are used

3. Extension to Two Measurement Association (TMA) Problem

In practice there may be limitations in the number of landmarks that one can use. Several reasons may contribute to this and include the cost of placing more landmarks, increase in image processing burden, occlusion in cluttered environment, or distant landmarks outside the visible range.

Having visual sensors, we have to deal with the possibility that only a small number of landmarks are visible by the robot at any given moment. However, as demonstrated in Section 2, localisation accuracy improves with the number of measurements. Therefore, if a vehicle can store more than one set of measurements at different locations and if these measurements can be combined in some way, then position estimation often becomes more accurate. This idea is explored in the next subsection.

3.1 Geometry Involving Two Successive Robot Positions

Figure 10 shows the vehicle's current position **B1** and its previous position **B2**. We assume that the path between **B2** and **B1** is circular (including straight, equivalent to infinite radius). The vehicle can generate a curved path via wheel steering [Green, D. N., et. al., 1993] or differentially driving the wheels [Chong, K. S., and Kleeman, L., 1997] [Papadopoulos, E., and Misailidis, M., 2007].

What we want to estimate is $\{\theta_1, X_T, Y_T\}$ at **B1** (refer to (2) for definition). As in Section 2.2, we use the measurements taken at **B1** to form the equation in (4). The next step is to correspond the measurements obtained from **B2** (ie., β_{2i}) to those collected at **B1**. To do so we introduce three additional parameters, d_{12}, $\Delta\theta$ and α (see Figure 10 and Figure 11) where (d_{12}, α) is the polar coordinate of **B2** with respect to **B1**, and $\Delta\theta$ reflects the curvature of the path. Mathematical derivations of these terms are given in Section 3.2.

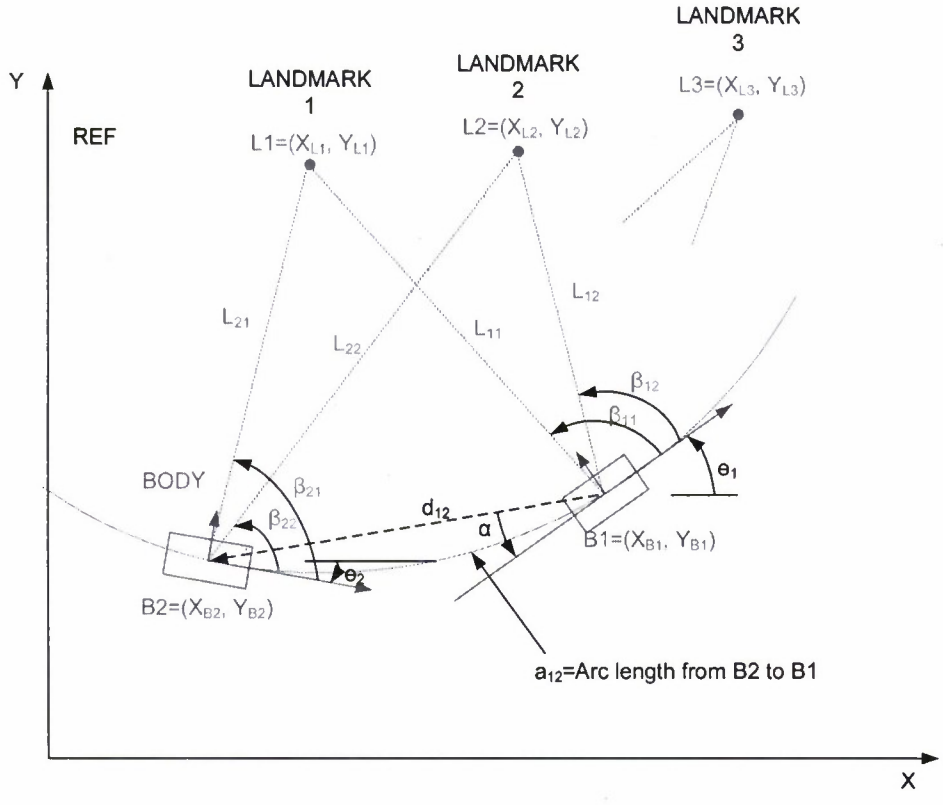

Figure 10: Illustration of a mobile robot moving from **B2** *to* **B1** *in 1 second interval. Rotation of* $\Delta\theta = \theta_1 - \theta_2$ *is the result of taking a circular path.*

3.2 Vehicle Odometry

We use Figure 11 to illustrate the basic geometry leading to the definition and derivation of the three terms $d_{12}, \Delta\theta$ and α. We approximate the path between two successive positions as circular. This also includes straight paths, which are circular with infinite radius.

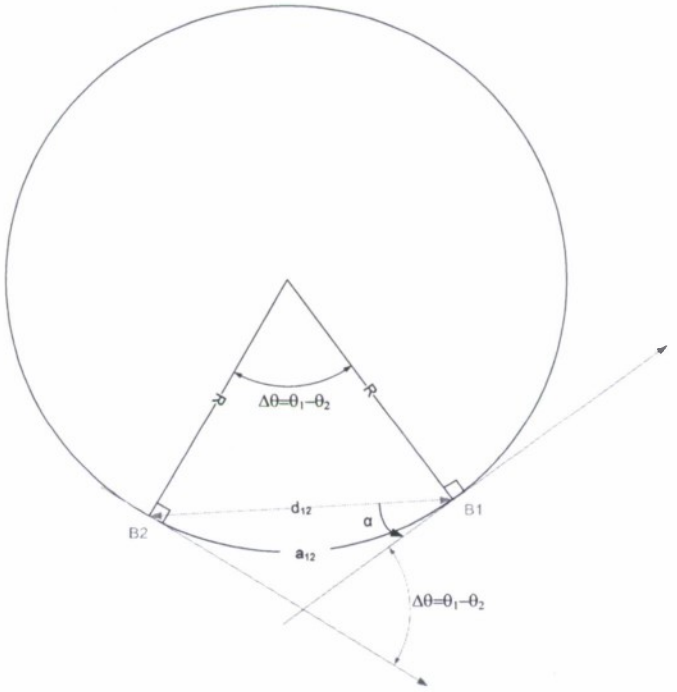

Figure 11: Definition of geometric terms between two successive vehicle positions - $d_{12}, \Delta\theta$ and α

The odometry terms are defined as below.

- a_{12} -arc length between **B1** and **B2** (circular arc),
- d_{12} - linear distance between **B1** and **B2**,
- α - look angle to **B2**, and
- $\Delta\theta = \theta_1 - \theta_2$ - rotation increment.

These terms can be deduced from either wheel steering angle (for steered vehicle) or wheel speeds (for differentially driven vehicle).

3.2.1 Wheel Steered Vehicle

Knowing the steering angle (ie., the control input), the turn radius R (in Figure 11) can be computed using $R = \frac{L}{\tan\gamma}$ where L and γ are the wheel base and steering angle respectively [Green, D. N., et. al., 1993]. Having computed R, the values for $d_{12}, \Delta\theta$ and α can be obtained as below.

$$\Delta\theta = \theta_1 - \theta_2 = \frac{a_{12}}{R}, \tag{15}$$

$$d_{12} = R\sqrt{2(1-\cos(\Delta\theta))} \text{ and} \tag{16}$$

$$\alpha = \frac{\Delta\theta}{2} \tag{17}$$

3.2.2 Differentially Driven Vehicle

For a differentially driven vehicle, the control input to the vehicle is $\mathbf{u} = [V_R, V_L]^T$, where V_R and V_L are the linear speeds of the right and left wheels. Assuming that V_R and V_L are constant within each time step, the dynamic equation of motion can be expressed as below [Chong, K. S., and Kleeman, L., 1997].

$$\begin{bmatrix} X_{B1} \\ Y_{B1} \\ \theta_1 \end{bmatrix} = \begin{bmatrix} X_{B2} \\ Y_{B2} \\ \theta_2 \end{bmatrix} + \begin{bmatrix} d_{12}\cos(\theta_2 - \alpha) \\ d_{12}\sin(\theta_2 - \alpha) \\ \Delta\theta \end{bmatrix} \tag{18}$$

where

$$\Delta\theta = \frac{V_R - V_L}{L}, \text{ where } L \text{ is wheelbase,} \tag{19}$$

$$d_{12} = \left(\frac{V_R + V_L}{2}\right)\Delta t \text{ and} \tag{20}$$

$$\alpha = \frac{\Delta\theta}{2}. \tag{21}$$

3.3 Problem Formulation

As in Section 2.2, for the current position **B1**, we have

$$\begin{bmatrix} A11_1 & A12_1 & \sin\beta_{11} & -\cos\beta_{11} \\ A11_2 & A12_2 & \sin\beta_{12} & -\cos\beta_{12} \\ \mathrm{M} & \mathrm{M} & \mathrm{M} & \mathrm{M} \\ A11_N & A12_N & \sin\beta_{1N} & -\cos\beta_{1N} \end{bmatrix} \cdot \begin{bmatrix} \cos\theta_1 \\ \sin\theta_1 \\ X_T \\ Y_T \end{bmatrix} = \mathbf{0}_{N\times 1} \tag{22}$$

where

$$A11_i = \sin\beta_{1i}X_{Li} - \cos\beta_{1i}Y_{Li} \tag{23}$$

$$A12_i = \sin\beta_{1i}Y_{Li} + \cos\beta_{1i}X_{Li} \tag{24}$$

Now consider the landmark position seen from the location **B2.**

$$\mathbf{L}_i^{B2} = \begin{bmatrix} L_{2i}\cos\beta_{2i} \\ L_{2i}\sin\beta_{2i} \end{bmatrix} = \mathbf{R}_{B1}^{B2}\mathbf{R}_R^{B1}(\mathbf{L}_i - \mathbf{B}_2) = \mathbf{R}_{B1}^{B2}\mathbf{R}_R^{B1}\mathbf{L}_i - \mathbf{R}_{B1}^{B2}\mathbf{R}_R^{B1}\mathbf{B}_2 \tag{25}$$

After some algebraic manipulations, we obtain

$$\begin{bmatrix} A21_i & A22_i & \sin\beta_{2i}c - \cos\beta_{2i}s & -\sin\beta_{2i}s - \cos\beta_{2i}c \end{bmatrix} \begin{bmatrix} \cos(\theta_1) \\ \sin(\theta_1) \\ X_T \\ Y_T \end{bmatrix} = m_i \tag{26}$$

where

$$A21_i = \left[\sin\beta_{2i}(cX_{Li} - sY_{Li}) + \cos\beta_{2i}(-sX_{Li} - cY_{Li})\right] \tag{27}$$

$$A22_i = \left[\sin\beta_{2i}(sX_{Li} + cY_{Li}) + \cos\beta_{2i}(cX_{Li} - sY_{Li})\right] \tag{28}$$

$$m_i = -\sin\beta_{2i}c \cdot d_{12}c_\alpha - \sin\beta_{2i}s \cdot d_{12}s_\alpha + \cos\beta_{2i}s \cdot d_{12}c_\alpha - \cos\beta_{2i}c \cdot d_{12}s_\alpha \tag{29}$$

In the absence of measurement errors, stacking up for all the landmarks gives

$$\begin{bmatrix} A21_1 & A22_1 & \sin\beta_{21}c - \cos\beta_{21}s & -\sin\beta_{21}s - \cos\beta_{21}c \\ A21_2 & A22_2 & \sin\beta_{22}c - \cos\beta_{22}s & -\sin\beta_{22}s - \cos\beta_{22}c \\ \mathrm{M} & \mathrm{M} & \mathrm{M} & \mathrm{M} \\ A21_N & A22_N & \sin\beta_{2N}c - \cos\beta_{2N}s & -\sin\beta_{2N}s - \cos\beta_{2N}c \end{bmatrix} \begin{bmatrix} \cos(\theta_1) \\ \sin(\theta_1) \\ X_T \\ Y_T \end{bmatrix} = \begin{bmatrix} m_1 \\ m_2 \\ \mathrm{M} \\ m_N \end{bmatrix} \tag{30}$$

The equations (22) and (30) can be combined in to $\mathbf{Ax} = \mathbf{b}$ where $\mathbf{A}$ is $2N \times 4$, $\mathbf{x}$ is 4×1 and $\mathbf{b}$ is $2N \times 1$ (see below).

$$\begin{bmatrix} A11_1 & A12_1 & \sin\beta_{11} & -\cos\beta_{11} \\ A11_2 & A12_2 & \sin\beta_{12} & -\cos\beta_{12} \\ \mathrm{M} & \mathrm{M} & \mathrm{M} & \mathrm{M} \\ A11_N & A12_N & \sin\beta_{1N} & -\cos\beta_{1N} \\ A21_1 & A22_1 & \sin\beta_{21}c - \cos\beta_{21}s & -\sin\beta_{21}s - \cos\beta_{21}c \\ A21_2 & A22_2 & \sin\beta_{22}c - \cos\beta_{22}s & -\sin\beta_{22}s - \cos\beta_{22}c \\ \mathrm{M} & \mathrm{M} & \mathrm{M} & \mathrm{M} \\ A21_N & A22_N & \sin\beta_{2N}c - \cos\beta_{2N}s & -\sin\beta_{2N}s - \cos\beta_{2N}c \end{bmatrix} \begin{bmatrix} \cos\theta_1 \\ \sin\theta_1 \\ X_T \\ Y_T \end{bmatrix} = \begin{bmatrix} 0 \\ 0 \\ \mathrm{M} \\ 0 \\ m_1 \\ m_2 \\ \mathrm{M} \\ m_N \end{bmatrix} \tag{31}$$

Note that $\Delta\theta$ is embedded in $\mathbf{A}$ and $\mathbf{b}$, and d_{12} and α are embedded in $\mathbf{b}$, effectively replacing **B2** parameters.

3.4 Optimal Solution

In presence of measurement errors, where $\mathbf{Ax} \cong \mathbf{b}$, our objective becomes

$$\boxed{\begin{array}{l}\text{Minimise} \quad \mathbf{x}^T\mathbf{P}\mathbf{x} + 2\mathbf{p}^T\mathbf{x} + u \\ \text{subject to} \quad \mathbf{x}^T\mathbf{Q}\mathbf{x} - 1 = 0\end{array}} \tag{32}$$

where $\mathbf{P} = \mathbf{A}^T\mathbf{A}$ (symmetric and positive definite), (33)

$\mathbf{p}^T = -\mathbf{b}^T\mathbf{A}$, (34)

$u = \mathbf{b}^T\mathbf{b}$ and (35)

$$\mathbf{Q} = \begin{bmatrix} 1 & 0 & 0 & 0 \\ 0 & 1 & 0 & 0 \\ 0 & 0 & 0 & 0 \\ 0 & 0 & 0 & 0 \end{bmatrix} \tag{36}$$

To solve this problem, we first transform (32) into a simpler form where $\mathbf{P}$ disappears from the quadratic term.

Since $\mathbf{P}$ and $\mathbf{Q}$ are symmetric, and $\mathbf{P}$ is positive definite, there exists a transformation matrix $\mathbf{S}$ that will transform $\mathbf{P}$ to $\mathbf{I}_{4\times4}$ and $\mathbf{Q}$ to a diagonal matrix. (ie., $\mathbf{SPS}^T = \mathbf{I}_{4\times4}$ and $\mathbf{SQS}^T = \mathbf{Q}_D$ (diagonal)). The proof is included in Appendix C.

$\mathbf{S}$ and $\mathbf{Q}_D$ are computed as follows:

1. $\mathbf{S}_1 = \mathbf{P}^{-\frac{1}{2}} = \mathbf{V}_\mathbf{P}\boldsymbol{\Sigma}_\mathbf{P}^{-\frac{1}{2}}\mathbf{V}_\mathbf{P}^T$ where $(\mathbf{V}_\mathbf{P}, \boldsymbol{\Sigma}_\mathbf{P}) = eig(\mathbf{P})$
2. Let $\mathbf{Y} = \mathbf{S}_1\mathbf{Q}\mathbf{S}_1^T$
3. $\mathbf{S}_2 = \mathbf{V}_\mathbf{Y}^T$ (eigenvectors of Y) where $(\mathbf{V}_\mathbf{Y}, \boldsymbol{\Sigma}_\mathbf{Y}) = eig(\mathbf{Y})$
4. $\mathbf{S} = \mathbf{S}_2\mathbf{S}_1$
5. $\mathbf{Q}_D = \mathbf{SQS}^T = \boldsymbol{\Sigma}_\mathbf{Y}$

Note $\mathbf{Q}_D$ and $\mathbf{Q}$ are congruent matrices, hence have the same inertia (ie., same number of positive, negative and zero eigenvalues). They both have 2 positive and 2 zero eigenvalues.

$$\mathbf{Q}_D = \begin{bmatrix} \mu_1 & 0 & 0 & 0 \\ 0 & \mu_2 & 0 & 0 \\ 0 & 0 & 0 & 0 \\ 0 & 0 & 0 & 0 \end{bmatrix} \text{ where } \mu_1 > \mu_2 \tag{37}$$

Then the objective function and constraint can be re-expressed as below.

$$\begin{aligned}&\mathbf{x}^T\mathbf{P}\mathbf{x}+2\mathbf{p}^T\mathbf{x}+u\\&=\mathbf{y}^T\mathbf{S}\mathbf{P}\mathbf{S}^T\mathbf{y}+2\mathbf{p}^T\mathbf{S}^T\mathbf{y}+u\text{, where }\mathbf{x}^T=\mathbf{y}^T\mathbf{S}\text{ and }\mathbf{x}=\mathbf{S}^T\mathbf{y}\\&=\mathbf{y}^T\mathbf{y}+2\mathbf{g}^T\mathbf{y}+u\text{, where }\mathbf{p}^T\mathbf{S}^T=\mathbf{g}^T\end{aligned} \tag{38}$$

$$\begin{aligned}&\mathbf{x}^T\mathbf{Q}\mathbf{x}-1\\&=\mathbf{y}^T\mathbf{S}\mathbf{Q}\mathbf{S}^T\mathbf{y}-1\\&=\mathbf{y}^T\mathbf{Q}_D\mathbf{y}-1=0\end{aligned} \tag{39}$$

Now define Lagrangian of the reduced problem as

$$L(\mathbf{y},\lambda)=\mathbf{y}^T\mathbf{y}+2\mathbf{g}^T\mathbf{y}+u-\lambda(\mathbf{y}^T\mathbf{Q}_D\mathbf{y}-1) \tag{40}$$

Setting the partial derivative terms to zero,

$$\frac{\partial L}{\partial \mathbf{y}}=2(\mathbf{y}+\mathbf{g}-\lambda\mathbf{Q}_D\mathbf{y})=2((\mathbf{I}-\lambda\mathbf{Q}_D)\mathbf{y}+\mathbf{g})=\mathbf{0} \tag{41}$$

$$\frac{\partial L}{\partial \lambda}=\mathbf{y}^T\mathbf{Q}_D\mathbf{y}-1=0 \tag{42}$$

From (41),

$$\mathbf{y}=-(\mathbf{I}-\lambda\mathbf{Q}_D)^{-1}\mathbf{g}=-\mathbf{D}_\lambda\mathbf{g} \tag{43}$$

where

$$\mathbf{D}_\lambda=(\mathbf{I}-\lambda\mathbf{Q}_D)^{-1}=\begin{bmatrix}\frac{1}{1-\lambda\mu_1} & 0 & 0 & 0\\ 0 & \frac{1}{1-\lambda\mu_2} & 0 & 0\\ 0 & 0 & 1 & 0\\ 0 & 0 & 0 & 1\end{bmatrix}=\mathbf{D}_\lambda^T \tag{44}$$

Substituting $\mathbf{y}=-\mathbf{D}_\lambda\mathbf{g}$ into (42),

$K(\lambda)=\dfrac{\partial L}{\partial \lambda}=\mathbf{g}^T\mathbf{D}_\lambda^T\mathbf{Q}_D\mathbf{D}_\lambda\mathbf{g}-1=0$ which can be simplified to

$$K(\lambda)=\frac{\mu_1 g_1^2}{(1-\lambda\mu_1)^2}+\frac{\mu_2 g_2^2}{(1-\lambda\mu_2)^2}-1=0 \tag{45}$$

This constraint function $K(\lambda)$ can be shown to be monotonously increasing for λ within the interval $\Lambda = \left[-\infty, \frac{1}{\mu_1}\right]$, by noting $\frac{dK(\lambda)}{d\lambda} > 0 \ \ \forall \ \lambda \in \Lambda$. Proof that the global minimum is within Λ is shown in Appendix D.

The above finding combined with $\lim_{\lambda \to (-\infty)} K(\lambda) = -1$ and $\lim_{\lambda \to \left(\frac{1}{\mu_1}\right)^-} K(\lambda) = +\infty$ suggests that $K(\lambda)$ has exactly one zero crossing within Λ.

We can use matlab function *fzero* to look for the zero crossing (ie., λ^*) in Λ.

```
K=@(L) C1^2/(M1*(1-L*M1)^2)+C2^2/(M2*(1-L*M2)^2)+(s-C1^2/M1-C2^2/M2);
L_op=fzero(K, 1/M1*0.999);
```

Having found the optimal Lagrange multiplier λ^*, the optimal state can be computed as follows.

$$\mathbf{y}^* = -(\mathbf{I} - \lambda^* \mathbf{Q}_D)^{-1}\mathbf{g}$$

$$\begin{bmatrix} \frac{-1}{1-\lambda^*\mu_1} & 0 & 0 & 0 \\ 0 & \frac{-1}{1-\lambda^*\mu_2} & 0 & 0 \\ 0 & 0 & -1 & 0 \\ 0 & 0 & 0 & -1 \end{bmatrix} \begin{bmatrix} g_1 \\ g_2 \\ g_3 \\ g_4 \end{bmatrix} = \begin{bmatrix} \frac{-g_1}{1-\lambda^*\mu_1} \\ \frac{-g_2}{1-\lambda^*\mu_2} \\ -g_3 \\ -g_4 \end{bmatrix} \tag{44}$$

$$\Rightarrow \mathbf{x}^* = \begin{bmatrix} \cos\theta_1^* \\ \sin\theta_1^* \\ X_T^* \\ Y_T^* \end{bmatrix} = \mathbf{S}^T\mathbf{y} \tag{45}$$

Optimal azimuths and positions are given below

$$\theta_1^* = \tan^{-1}(x^*(2)/x^*(1)) \text{ (matlab function "}atan2\text{(x(2), x(1))")} \tag{46}$$
$$\theta_2^* = \theta_1^* - \Delta\theta$$

$$\mathbf{B}_1^* = \begin{bmatrix} X_{B1}^* \\ Y_{B1}^* \end{bmatrix} = -\left[\mathbf{R}_R^{B1}\right]^T \begin{bmatrix} X_T^* \\ Y_T^* \end{bmatrix} \tag{47}$$

$$\mathbf{B}_2^* = \begin{bmatrix} X_{B2}^* \\ Y_{B2}^* \end{bmatrix} = \mathbf{B}_1^* + \begin{bmatrix} d_{12}\cos(\pi + \theta_1^* + \alpha) \\ d_{12}\sin(\pi + \theta_1^* + \alpha) \end{bmatrix} \quad (48)$$

3.5 Experimental Result

3.5.1 Default Scenario

The followings are the default settings used in the simulation.

- landmark positions: L={(0, 0), (40, 0), (0, 40), (40, 40)}
- speed=5m/s, wheel steering angle=5°, wheel base=0.5m, Δt =1sec.
- **B2**=(4, 10)m (start), **B1**= (7.7, 13.1)m (end);
- θ_2=15° (start), θ_1 =65.1273° (end),
- $d_{12} = 4.83\text{m}, \Delta\theta = 50.13°, \alpha = 25.06°$

The relative geometry terms have Gaussian noises as below:

- $\sigma(d_{12})$=0.25m (5% error),
- $\sigma(\Delta\theta)$=1° and
- $\sigma(\alpha)$=1°.

Default measurement noise is

- $\sigma(\beta_i) = 3°$ for each bearing.

3.5.2 Comparison with GED method

The measurement noise is varied from 0.5° to 10°. In Figure 12, position error (ie., $\sqrt{x\_err^2 + y\_err^2}$) and azimuth errors from the GED (blue) and TMA (green) methods are compared.

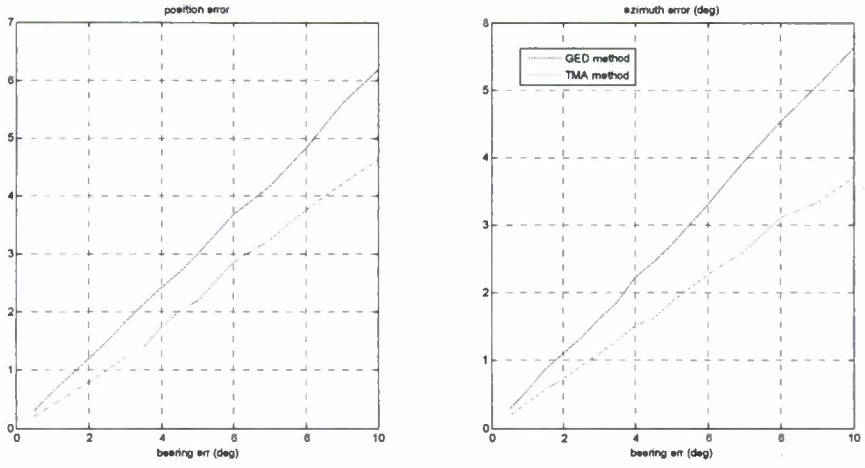

Figure 12: Position and azimuth error curves by GED (blue) and TMA (red).

It was previously shown in Figure 8 that the GED (with MLE) error curves are already close to the CRLB, indicating not much room for improvement. To go beyond the bounds, we somehow need to generate more measurements from the given number of landmarks, which is the underlying idea of the TMA approach. Having implemented this approach, the error curves for the TMA method (red) are significantly lower than the blue curves, and the estimation improvement of 25% and 35% are achieved for the position and azimuth respectively.

With the default setting of 3° bearing error, the position and azimuth errors are 1.2m (1σ) and 1° (1σ) respectively, and they increase linearly, reaching 4.5m and 3.7° at 10° bearing error. The difference between the GED and TMA errors are also presented in Figure 13 for a closer look.

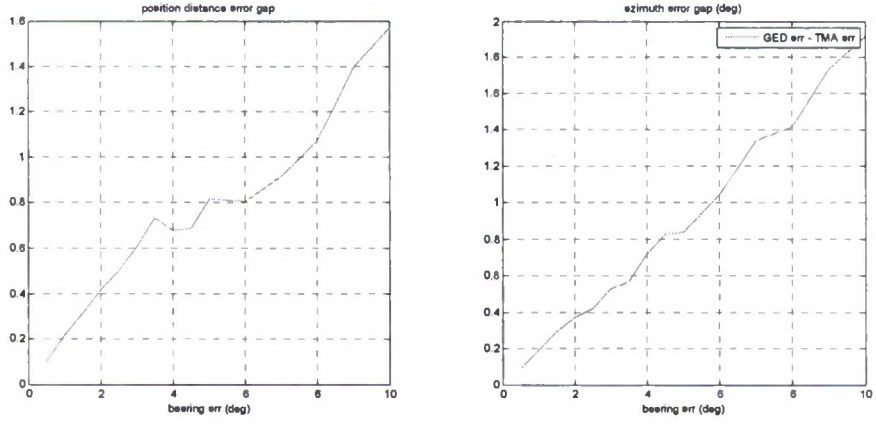

Figure 13: Difference of position and azimuth errors between the GED and TMA methods

3.5.3 Sensitivity to Odometry Errors

The TMA method requires known relative geometry between two successive positions in terms of $d_{12}, \Delta\theta$ and α. They can be provided by either odometry or inertial navigation system (INS). As for odometry, the error sources include mechanical imperfections, sensor errors, and wheel skidding or slippage.

For indoor applications, after calibration, positional accuracy can be as low as 1-2% of distance travelled [Papadopoulos, E., and Misailidis, M., 2007]. Setting the values for d_{12} and α errors should reflect such positional accuracy. According to [Borenstein, J., et al, 1996], $\Delta\theta$ error can be as low as 1-2° on smooth surface but can grow up to 8° with 10 bumps. This error growth can be prevented if a gyroscope is incorporated on the vehicle. We want to explore the sensitivity of the system to the errors associated with these parameters. We vary one parameter at a time, while keeping the other two at default values as in Subsection 3.5.1.

First, we vary the d_{12} error from 1% to 50% of the distance travelled (ie., 5m). Therefore 2.5m (1σ) would be the largest d_{12} error here. After 3000 Monte-Carlo simulations, the x/y position and azimuth errors are plotted against the d_{12} error in Figure 14. The red curves are the smallest possible estimation errors with 4 bearing measurements.

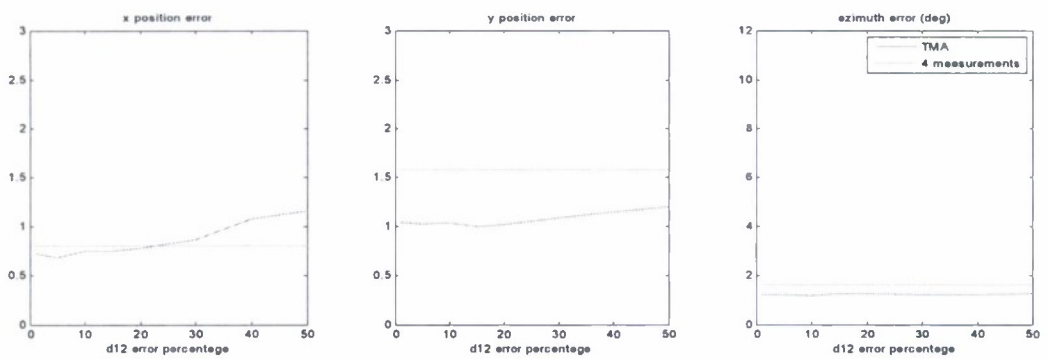

Figure 14: Estimation errors versus d_{12} error - red curves are the smallest possible estimation errors with 4 bearing measurements

It is shown that position errors remain steady for d_{12} error below 20% and increases when this error exceeds 20%. The increase in the displacement errors due to increase in the d_{12} error from 5% to 50% is about 0.63m (1σ). The azimuth accuracy does not seem to be affected by d_{12} error.

Next, we vary $\Delta\theta$ error from 1° to 30° while keeping the rest at default. The results shown in Figure 15 indicate that the performance is indeed sensitive to $\Delta\theta$ error. The blue curves grow rapidly from the start. The azimuth error exceeds the red curve at 2°, and the position error (x and y combined) exceeds the red bound at 12° bearing error (not shown in the figure). To keep

this error source under control in outdoor applications, external aiding such as gyroscope may be necessary.

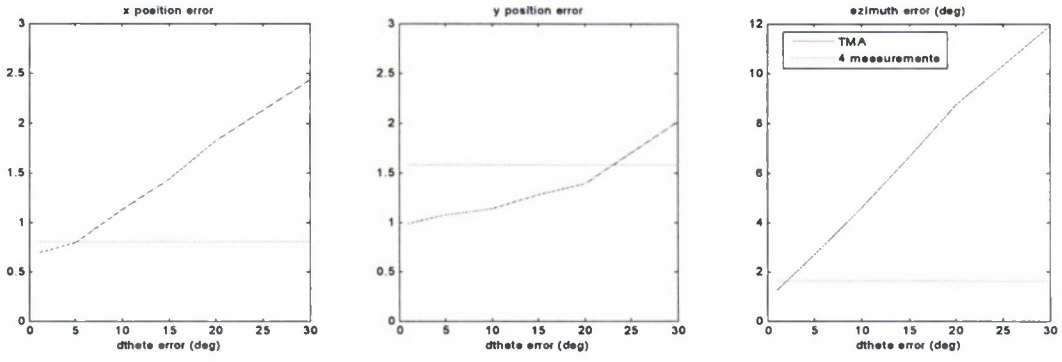

Figure 15: Estimation errors versus $\Delta\theta$ error (1σ) - red curves are the smallest possible estimation errors with 4 bearing measurements

Lastly, we vary α error from 1° to 30° while keeping the other two at default. According to Figure 16, α error contributes to position estimation errors but at a slower pace than $\Delta\theta$ error does. The azimuth error seems unaffected by α error. It appears that α error up to 10° may be well tolerated.

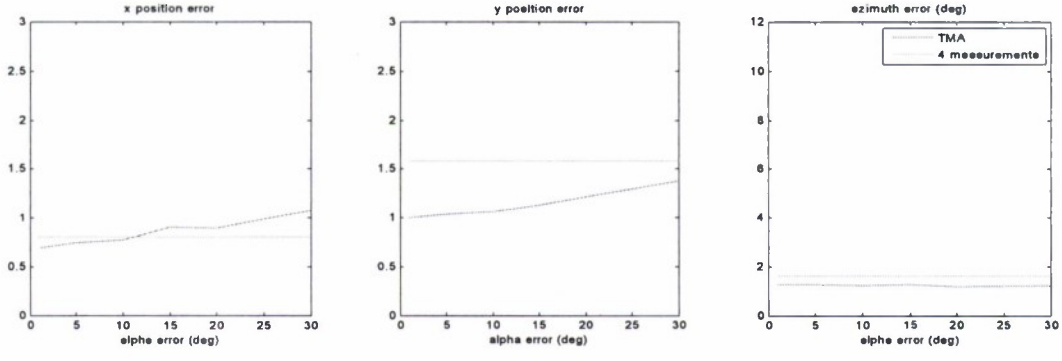

Figure 16: Estimation errors versus α error (1σ) - red curves are the smallest possible estimation errors with 4 bearing measurements

From the above observations, it is clear that incremental rotation $\Delta\theta$ is the most critical contributor to the localisation accuracy. It appears that $\Delta\theta$ error should be maintained below 2°. This can be achieved as numerous low cost gyroscopes in the market meet this requirement.

3.5.4 Sensitivity to Vehicle Speed

In this subsection, we examine the effect of distance travelled within one time step (ie., speed) on the estimation accuracy. The vehicle starts from (4, 10) with zero azimuth. It moves straight by a distance of d_{12}, which varies from 0.1m to 30m. Just for this test, we set the d_{12}, $\Delta\theta$ and α errors to zero, and bearing error to $3°\,(1\sigma)$.

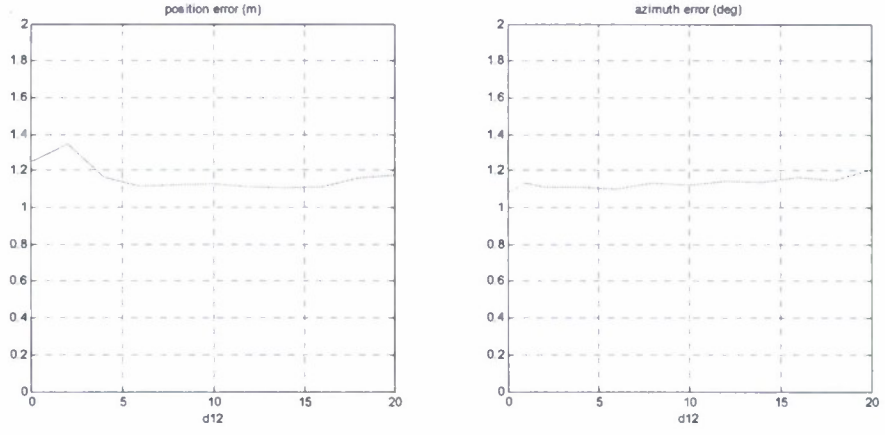

Figure 17: Estimation errors versus distance travelled within the time step

After 3000 Monte-Carlo simulations, the position and azimuth errors are plotted versus the distance travelled (ie., d_{12}) in Figure 17. The estimation errors do not seem to vary much with d_{12}. The position error is larger for $d_{12} \leq 3$ m, and then remains small until d_{12} exceeds 16m. The azimuth error increases as d_{12} increases but the change is not significant. Therefore, we conclude that the speed variation during the mission does not affect the navigation accuracy.

4. Conclusions

We proposed two algorithms for estimating the position and orientation of a mobile robot (UGV) given noisy bearing measurements. The key findings of the study are listed below.

- The GED method finds the global minimum analytically and the estimation accuracy is close to the CRLB for bearing errors up to about 5°.
- If the bearing error becomes large (e.g., >5°), few iterations of MLE optimisation can be added to bring the estimates closer to the correct solution. This works more effectively when N is large.
- The performance is usually more accurate when the vehicle is within the area delimited by the landmarks.
- The TMA method makes use of additional bearing measurements collected at the previous unknown location, and finds the current and previous positions (and azimuths) simultaneously.
- The TMA method results in a significant improvement ($\approx 30\%$) by effectively doubling the number of the measurements.
- The TMA method requires three additional terms, $d_{12}, \Delta\theta$ and α, and shows greatest sensitivity to $\Delta\theta$ error. For outdoor applications, incorporation of a gyroscope with a bias below $1°/s$ is recommended.
- The vehicle speed does not significantly affect the performance.

These methods, especially TMA, can be combined with inertial navigation system (INS) where the INS can provide accurate estimates of $d_{12}, \Delta\theta$ and α, and the TMA can prevent the INS solution from drifting via Kalman filtering.

The authors are currently investigating the 3D localisation problem, where the vehicle (either UAV or UGV) has a moderate tilt and takes measurements in azimuth and elevation.

5. References

1. Betke, M., and Gurvits, L., "Mobile Robot Localization Using Landmarks", "IEEE Transactions of Robotics and Automation, Vol. 13, No. 2, April 1997, pg 251-263.
2. Borenstein, J., Everett, H. R., Feng, L., and Wehe, D., "Mobile Robot Positioning: Sensors and Techniques", Journal of Robotic Sytems Vol. 14, No. 4, pg 231-249, 1997.
3. Chong, K. S., and Kleeman, L., "Accurate Odometry and Error Modeling for a Mobile Robot", In IEEE International Conference on Robotics & Automation, 1997, pg 2783-2788.
4. Daniilidis, K., "The Page of Omni-directional Vision", www.cis.upenn.edu /~kostas/omni.html maintained by GRASP Laboratory.
5. Green, D. N., Sasiadek, J. Z., and Vukovich, G. S., "Guidance and Control of an Autonomous Planetary Rover", IEEE - IEE Vehicle Navigation and Information Systems Conference, Ottawa - VNIS'93, 1993, pg 539-542.
6. Papadopoulos, E., and Misailidis, M., "On Differential Drive Robot Odometry with Application to Path Planning", Proceedings of the European Control Conference, 2007, Kos, Greece, July 2-5, 2007, pg 5492-5499
7. Shimshoni, I., "On Mobile Robot Localization from Landmark Bearings", IEEE Transactions on Robotics and Automation, Vol. 18, No. 6, December 2002, pg 971-976.
8. Torrieri, D. J., "Statistical Theory of Passive Location Systems", IEEE Transactions on Aerospace and Electronic Systems, Vol. AES-20, No. 2, March 1984, pg 183-198.

6. Acknowledgement

Authors would like to thank Dr. Farhan Faruqi (Head of Guidance and Control Group) for his kind support on this work.

THIS PAGE HAS BEEN
INTENTIONALLY LEFT BLANK

Appendix A: Detailed Derivation of TMA Method

Rotation Matrices:

$$\mathbf{R}_R^{B1} = \begin{bmatrix} \cos\theta_1 & \sin\theta_1 \\ -\sin\theta_1 & \cos\theta_1 \end{bmatrix} = \begin{bmatrix} c_1 & s_1 \\ -s_1 & c_1 \end{bmatrix} \text{ REF to Robot Position 1 (at current time)}$$

$$\mathbf{R}_R^{B2} = \begin{bmatrix} \cos\theta_2 & \sin\theta_2 \\ -\sin\theta_2 & \cos\theta_2 \end{bmatrix} = \begin{bmatrix} c_2 & s_2 \\ -s_2 & c_2 \end{bmatrix} \text{ REF to Robot Position 2 (at previous time)}$$

$$\mathbf{R}_{B2}^{B1} = \begin{bmatrix} \cos(\Delta\theta) & \sin(\Delta\theta) \\ -\sin(\Delta\theta) & \cos(\Delta\theta) \end{bmatrix} = \begin{bmatrix} c & s \\ -s & c \end{bmatrix} \text{ Robot Position 2 to Robot Position1}$$

For Robot Position 1 (Current Time): Consider i^{th} landmark position L_i wrt B1 frame

$$\mathbf{L}_i^{B1} = \begin{bmatrix} L_{1i}\cos\beta_{1i} \\ L_{1i}\sin\beta_{1i} \end{bmatrix} = \mathbf{R}_R^{B1}(\mathbf{L}_i - \mathbf{B}_1) = \mathbf{R}_R^{B1}\mathbf{L}_i - \mathbf{R}_R^{B1}\mathbf{B}_1 = \begin{bmatrix} \cos\theta_1 & \sin\theta_1 \\ -\sin\theta_1 & \cos\theta_1 \end{bmatrix}\begin{bmatrix} X_{Li} \\ Y_{Li} \end{bmatrix} + \mathbf{T}_1^{B1} \quad \text{(A1)}$$

where $\mathbf{T}_1^{B1} = \begin{bmatrix} X_T \\ Y_T \end{bmatrix} = -\mathbf{R}_R^{B1}\mathbf{B}_1$

Diving the top row by bottom row,

$$\frac{\cos\beta_{1i}}{\sin\beta_{1i}} = \frac{\cos\theta_1 X_{Li} + \sin\theta_1 Y_{Li} + X_T}{-\sin\theta_1 X_{Li} + \cos\theta_1 Y_{Li} + Y_T}$$

$$\sin\beta_{1i}(\cos\theta_1 X_{Li} + \sin\theta_1 Y_{Li} + X_T) - \cos\beta_{1i}(-\sin\theta_1 X_{Li} + \cos\theta_1 Y_{Li} + Y_T) = 0$$

$$\left[\sin\beta_{1i}X_{Li} - \cos\beta_{1i}Y_{Li},\quad \sin\beta_{1i}Y_{Li} + \cos\beta_{1i}X_{Li},\quad \sin\beta_{1i},\quad -\cos\beta_{1i}\right]\cdot\begin{bmatrix} \cos\theta_1 \\ \sin\theta_1 \\ X_T \\ Y_T \end{bmatrix} = 0 \quad \text{(A2)}$$

Let

$$Al1_i = \sin\beta_{1i}X_{Li} - \cos\beta_{1i}Y_{Li}$$

$$Al2_i = \sin\beta_{1i}Y_{Li} + \cos\beta_{1i}X_{Li}$$

For n landmarks,

$$\begin{bmatrix} A11_1 & A12_1 & \sin\beta_{11} & -\cos\beta_{11} \\ A11_2 & A12_2 & \sin\beta_{12} & -\cos\beta_{12} \\ \mathrm{M} & \mathrm{M} & \mathrm{M} & \mathrm{M} \\ A11_N & A12_N & \sin\beta_{1N} & -\cos\beta_{1N} \end{bmatrix} \cdot \begin{bmatrix} \cos\theta_1 \\ \sin\theta_1 \\ X_T \\ Y_T \end{bmatrix} = \mathbf{0}_{N\times 1} \tag{A3}$$

For Robot Position 2 (previous time step): Consider i[th] landmark position $\mathbf{L}_i$ wrt B2 frame

$$\mathbf{L}_i^{B2} = \begin{bmatrix} L_{2i}\cos\beta_{2i} \\ L_{2i}\sin\beta_{2i} \end{bmatrix} = \mathbf{R}_{B1}^{B2}\mathbf{R}_R^{B1}\left(\mathbf{L}_i - \mathbf{B}_2\right) = \mathbf{R}_{B1}^{B2}\mathbf{R}_R^{B1}\mathbf{L}_i - \mathbf{R}_{B1}^{B2}\mathbf{R}_R^{B1}\mathbf{B}_2 \tag{A4}$$

$$= \mathbf{R}_{B1}^{B2}\mathbf{R}_R^{B1}\mathbf{L}_i - \mathbf{R}_{B1}^{B2}\mathbf{R}_R^{B1}\left(\mathbf{B}_1 + \mathbf{R}_{B1}^{R}\left[\mathbf{B}_2 - \mathbf{B}_1\right]^{B1}\right)$$

$$= \mathbf{R}_{B1}^{B2}\mathbf{R}_R^{B1}\mathbf{L}_i - \mathbf{R}_{B1}^{B2}\mathbf{R}_R^{B1}\left(\mathbf{B}_1 + \mathbf{R}_{B1}^{R}\begin{bmatrix} -d_{12}\cos\alpha \\ d_{12}\sin\alpha \end{bmatrix}\right)$$

$$= \mathbf{R}_{B1}^{B2}\mathbf{R}_R^{B1}\mathbf{L}_i - \mathbf{R}_{B1}^{B2}\mathbf{R}_R^{B1}\begin{bmatrix} X_{B1} \\ Y_{B1} \end{bmatrix} - \mathbf{R}_{B1}^{B2}\begin{bmatrix} -d_{12}\cos\alpha \\ d_{12}\sin\alpha \end{bmatrix}$$

$$= \mathbf{R}_{B1}^{B2}\mathbf{R}_R^{B1}\mathbf{L}_i + \mathbf{R}_{B1}^{B2}\begin{bmatrix} X_T \\ Y_T \end{bmatrix} - \mathbf{R}_{B1}^{B2}\begin{bmatrix} -d_{12}\cos\alpha \\ -d_{12}\sin\alpha \end{bmatrix}, \text{ where } \begin{bmatrix} X_T \\ Y_T \end{bmatrix} = -\mathbf{R}_R^{B1}\mathbf{B}_1$$

$$= \begin{bmatrix} c & -s \\ s & c \end{bmatrix}\begin{bmatrix} \cos\theta_1 & \sin\theta_1 \\ -\sin\theta_1 & \cos\theta_1 \end{bmatrix}\begin{bmatrix} X_{Li} \\ Y_{Li} \end{bmatrix} + \begin{bmatrix} c & -s \\ s & c \end{bmatrix}\begin{bmatrix} X_T \\ Y_T \end{bmatrix} - \begin{bmatrix} c & -s \\ s & c \end{bmatrix}\begin{bmatrix} -d_{12}\cos\alpha \\ d_{12}\sin\alpha \end{bmatrix}$$

$$= \begin{bmatrix} c\cdot\cos\theta_1 + s\cdot\sin\theta_1 & c\cdot\sin\theta_1 - s\cdot\cos\theta_1 \\ s\cdot\cos\theta_1 - c\cdot\sin\theta_1 & s\cdot\sin\theta_1 + c\cdot\cos\theta_1 \end{bmatrix}\begin{bmatrix} X_{Li} \\ Y_{Li} \end{bmatrix} + \begin{bmatrix} cX_T - sY_T \\ sX_T + cY_T \end{bmatrix} - \begin{bmatrix} -c\cdot d_{12}\cos\alpha - s\cdot d_{12}\sin\alpha \\ -s\cdot d_{12}\cos\alpha + c\cdot d_{12}\sin\alpha \end{bmatrix}$$

Using shorthand notation for sine and cosine functions,

$$= \begin{bmatrix} c\cdot c_1 + s\cdot s_1 & c\cdot s_1 - s\cdot c_1 \\ s\cdot c_1 - c\cdot s_1 & s\cdot s_1 + c\cdot c_1 \end{bmatrix}\begin{bmatrix} X_{Li} \\ Y_{Li} \end{bmatrix} + \begin{bmatrix} cX_T - sY_T \\ sX_T + cY_T \end{bmatrix} - \begin{bmatrix} -c\cdot d_{12}c_\alpha - s\cdot d_{12}s_\alpha \\ -s\cdot d_{12}c_\alpha + c\cdot d_{12}s_\alpha \end{bmatrix} \tag{A5}$$

Dividing the first row by second row,

$$\frac{L_{2i}\cos\beta_{2i}}{L_{2i}\sin\beta_{2i}} = \frac{(c\cdot c_1 + s\cdot s_1)X_{Li} + (c\cdot s_1 - s\cdot c_1)Y_{Li} + cX_T - sY_T + c\cdot d_{12}c_\alpha + s\cdot d_{12}s_\alpha}{(s\cdot c_1 - c\cdot s_1)X_{Li} + (s\cdot s_1 + c\cdot c_1)Y_{Li} + sX_T + cY_T + s\cdot d_{12}c_\alpha - c\cdot d_{12}s_\alpha}$$

$$\sin\beta_{2i}\left[(c\cdot c_1+s\cdot s_1)X_{Li}+(c\cdot s_1-s\cdot c_1)Y_{Li}+cX_T-sY_T+c\cdot d_{12}c_\alpha+s\cdot d_{12}s_\alpha\right]$$
$$-\cos\beta_{2i}\left[(s\cdot c_1-c\cdot s_1)X_{Li}+(s\cdot s_1+c\cdot c_1)Y_{Li}+sX_T+cY_T+s\cdot d_{12}c_\alpha-c\cdot d_{12}s_\alpha\right]=0$$

$$\sin\beta_{2i}(c\cdot c_1+s\cdot s_1)X_{Li}+\sin\beta_{2i}(c\cdot s_1-s\cdot c_1)Y_{Li}-\cos\beta_{2i}(s\cdot c_1-c\cdot s_1)X_{Li}-\cos\beta_{2i}(s\cdot s_1+c\cdot c_1)Y_{Li}$$
$$+\sin\beta_{2i}cX_T-\cos\beta_{2i}sX_T-\sin\beta_{2i}sY_T-\cos\beta_{2i}cY_T$$
$$+\sin\beta_{2i}c\cdot d_{12}c_\alpha+\sin\beta_{2i}s\cdot d_{12}s_\alpha-\cos\beta_{2i}s\cdot d_{12}c_\alpha+\cos\beta_{2i}c\cdot d_{12}s_\alpha=0$$

$$\left[\sin\beta_{2i}(cX_{Li}-sY_{Li})+\cos\beta_{2i}(-sX_{Li}-cY_{Li})\right]c_1+\left[\sin\beta_{2i}(sX_{Li}+cY_{Li})+\cos\beta_{2i}(cX_{Li}-sY_{Li})\right]s_1$$
$$+\left[\sin\beta_{2i}c-\cos\beta_{2i}s\right]X_T+\left[-\sin\beta_{2i}s-\cos\beta_{2i}c\right]Y_T$$
$$-\left[-\sin\beta_{2i}c\cdot d_{12}c_\alpha-\sin\beta_{2i}s\cdot d_{12}s_\alpha+\cos\beta_{2i}s\cdot d_{12}c_\alpha-\cos\beta_{2i}c\cdot d_{12}s_\alpha\right]=0$$

Let

$$A21_i=\left[\sin\beta_{2i}(cX_{Li}-sY_{Li})+\cos\beta_{2i}(-sX_{Li}-cY_{Li})\right]$$
$$A22_i=\left[\sin\beta_{2i}(sX_{Li}+cY_{Li})+\cos\beta_{2i}(cX_{Li}-sY_{Li})\right]$$
$$m_i=-\sin\beta_{2i}c\cdot d_{12}c_\alpha-\sin\beta_{2i}s\cdot d_{12}s_\alpha+\cos\beta_{2i}s\cdot d_{12}c_\alpha-\cos\beta_{2i}c\cdot d_{12}s_\alpha$$

Then $$\begin{bmatrix}A21_i & A22_i & \sin\beta_{2i}c-\cos\beta_{2i}s & -\sin\beta_{2i}s-\cos\beta_{2i}c\end{bmatrix}\begin{bmatrix}\cos(\theta_1)\\ \sin(\theta_1)\\ X_T\\ Y_T\end{bmatrix}=m_i \qquad \text{(A6)}$$

Stacking up rows for all the landmarks

$$\begin{bmatrix}A21_1 & A22_1 & \sin\beta_{21}c-\cos\beta_{21}s & -\sin\beta_{21}s-\cos\beta_{21}c\\ A21_2 & A22_2 & \sin\beta_{22}c-\cos\beta_{22}s & -\sin\beta_{22}s-\cos\beta_{22}c\\ \text{M} & \text{M} & \text{M} & \text{M}\\ A21_N & A22_N & \sin\beta_{2N}c-\cos\beta_{2N}s & -\sin\beta_{2N}s-\cos\beta_{2N}c\end{bmatrix}\begin{bmatrix}\cos(\theta_1)\\ \sin(\theta_1)\\ X_T\\ Y_T\end{bmatrix}=\begin{bmatrix}m_1\\ m_2\\ \text{M}\\ m_N\end{bmatrix} \qquad \text{(A7)}$$

The highlighted equations for B1 and B2 can be combined in to
Ax = b where **A** is $2N\times 4$, **x** is 4×1 and **b** is $2N\times 1$.

$$\begin{bmatrix}A11_1 & A12_1 & \sin\beta_{11} & -\cos\beta_{11}\\ A11_2 & A12_2 & \sin\beta_{12} & -\cos\beta_{12}\\ \text{M} & \text{M} & \text{M} & \text{M}\\ A11_N & A12_N & \sin\beta_{1N} & -\cos\beta_{1N}\\ A21_1 & A22_1 & \sin\beta_{21}c-\cos\beta_{21}s & -\sin\beta_{21}s-\cos\beta_{21}c\\ A21_2 & A22_2 & \sin\beta_{22}c-\cos\beta_{22}s & -\sin\beta_{22}s-\cos\beta_{22}c\\ \text{M} & \text{M} & \text{M} & \text{M}\\ A21_N & A22_N & \sin\beta_{2N}c-\cos\beta_{2N}s & -\sin\beta_{2N}s-\cos\beta_{2N}c\end{bmatrix}\begin{bmatrix}\cos\theta_1\\ \sin\theta_1\\ X_T\\ Y_T\end{bmatrix}=\begin{bmatrix}0\\ 0\\ \text{M}\\ 0\\ m_1\\ m_2\\ \text{M}\\ m_N\end{bmatrix} \qquad \text{(A8)}$$

THIS PAGE HAS BEEN
INTENTIONALLY LEFT BLANK

Appendix B: Maximum Likelihood Estimator

As mentioned in Section 2.6, $\mathbf{f(x)}$ is a nonlinear vector function. To determine a simple estimator, $\mathbf{f(x)}$ can be linearised as below

$$\mathbf{f(x)} \approx \mathbf{f(x_0)} + \mathbf{G} \cdot (\mathbf{x} - \mathbf{x}_0) \tag{B1}$$

where $\mathbf{G}$ is $N \times 3$ matrix of derivatives evaluated at $\mathbf{x}_0$.

$$\mathbf{G} = \begin{bmatrix} \left.\frac{\partial f_1}{\partial \mathbf{x}(1)}\right|_{\mathbf{x}=\mathbf{x}_0} & \left.\frac{\partial f_1}{\partial \mathbf{x}(2)}\right|_{\mathbf{x}=\mathbf{x}_0} & \left.\frac{\partial f_1}{\partial \mathbf{x}(3)}\right|_{\mathbf{x}=\mathbf{x}_0} \\ \mathrm{M} & \mathrm{M} & \mathrm{M} \\ \left.\frac{\partial f_N}{\partial \mathbf{x}(1)}\right|_{\mathbf{x}=\mathbf{x}_0} & \left.\frac{\partial f_N}{\partial \mathbf{x}(2)}\right|_{\mathbf{x}=\mathbf{x}_0} & \left.\frac{\partial f_N}{\partial \mathbf{x}(3)}\right|_{\mathbf{x}=\mathbf{x}_0} \end{bmatrix} \tag{B2}$$

The i^{th} bearing angle is expressed as

$$f_i(\mathbf{x}) = \tan^{-1}\left(\frac{g_y}{g_x}\right) \text{ where} \tag{B3}$$

$$g_x = \cos\theta(X_{Li} - X_B) + \sin\theta(Y_{Li} - Y_B)$$

$$g_y = -\sin\theta(X_{Li} - X_B) + \cos\theta(Y_{Li} - Y_B).$$

Then the i^{th} row elements of $\mathbf{G}$ are

$$\left.\frac{\partial f_i}{\partial \mathbf{x}(1)}\right|_{\mathbf{x}=\mathbf{x}_0} = \left.\frac{\partial f_i}{\partial \theta}\right|_{\mathbf{x}=\mathbf{x}_0} = \frac{-(g_x^2 + g_y^2)}{g_x^2 + g_y^2} = -1 \tag{B4}$$

$$\left.\frac{\partial f_i}{\partial \mathbf{x}(2)}\right|_{\mathbf{x}=\mathbf{x}_0} = \left.\frac{\partial f_i}{\partial X_B}\right|_{\mathbf{x}=\mathbf{x}_0} = \frac{\sin\theta_i g_x + g_y \cos\theta_i}{g_x^2 + g_y^2} \tag{B5}$$

$$\left.\frac{\partial f_i}{\partial \mathbf{x}(3)}\right|_{\mathbf{x}=\mathbf{x}_0} = \left.\frac{\partial f_i}{\partial Y_B}\right|_{\mathbf{x}=\mathbf{x}_0} = \frac{-\cos\theta_i g_x + g_y \sin\theta_i}{g_x^2 + g_y^2} \tag{B6}$$

Inserting (B1) into the cost function $\mathbf{Q(x)} = \left[\hat{\boldsymbol{\beta}} - \mathbf{f(x)}\right]^T \mathbf{N}^{-1}\left[\hat{\boldsymbol{\beta}} - \mathbf{f(x)}\right]$, (where $\mathbf{N}$ is a $N \times N$ measurement covariance matrix),

$$\mathbf{Q(x)} = \left[\hat{\boldsymbol{\beta}} - \mathbf{f(x_0)} - \mathbf{G(x - x_0)}\right]^T \mathbf{N}^{-1}\left[\hat{\boldsymbol{\beta}} - \mathbf{f(x_0)} - \mathbf{G(x - x_0)}\right]. \tag{B7}$$

To minimise $\mathbf{Q(x)}$, we want $\frac{\partial \mathbf{Q(x)}}{\partial \mathbf{x}} = \mathbf{0}_{3\times 1}$,

$$\frac{\partial \mathbf{Q(x)}}{\partial \mathbf{x}} = 2\mathbf{G}^T\mathbf{N}^{-1}\mathbf{G}\hat{\mathbf{x}} - 2\mathbf{G}^T\mathbf{N}^{-1}(\hat{\boldsymbol{\beta}} - \mathbf{f}(\hat{\mathbf{x}}_0) + \mathbf{G}\hat{\mathbf{x}}_0) = \mathbf{0}_{3\times 1} \tag{B8}$$

Rearranging (B8) gives the iterative estimation equation.

$$\hat{\mathbf{x}} = \hat{\mathbf{x}}_0 + \left(\mathbf{G}^T\mathbf{N}^{-1}\mathbf{G}\right)^{-1}\mathbf{G}^T\mathbf{N}^{-1}(\hat{\boldsymbol{\beta}} - \mathbf{f}(\hat{\mathbf{x}}_0) \tag{B9}$$

And if we assume $E[\hat{\mathbf{x}}] = \mathbf{x}$ (unbiased), then it can be shown that the covariance matrix of $\hat{\mathbf{x}}$ can be expressed as

$$\mathbf{P} = E[(\hat{\mathbf{x}} - E[\hat{\mathbf{x}}])(\hat{\mathbf{x}} - E[\hat{\mathbf{x}}])^T] = \left(\mathbf{G}^T\mathbf{N}^{-1}\mathbf{G}\right)^{-1}. \tag{B10}$$

The square-root of diagonals of $\mathbf{P}$ become the Cramer Rao Lower Bounds for the estimate accuracy of $\hat{\mathbf{x}} = [\hat{\theta}, \hat{X}_B, \hat{Y}_B]^T$.

Appendix C: Proof of Simultaneous Diagonalisation

Note $\mathbf{P}$ and $\mathbf{Q}$ are real symmetric, and $\mathbf{P}$ is positive definite. We define the matrices of eigenvectors and eigenvalues of $\mathbf{P}$ as $[\mathbf{V_P}, \mathbf{\Sigma_P}] = eig(\mathbf{P})$ where *eig* is a matlab function that produces a diagonal matrix $\mathbf{\Sigma_P}$ of eigenvalues and a full matrix $\mathbf{V_P}$ whose columns are the corresponding eigenvectors so that

$$\mathbf{V}_P^T \mathbf{P} \mathbf{V_P} = \mathbf{\Sigma_P}. \tag{C1}$$

We define a transformation matrix that will diagonalise $\mathbf{P}$ and $\mathbf{Q}$ simultaneously as product of two matrices.

$$\mathbf{S} = \mathbf{S}_2 \mathbf{S}_1. \tag{C2}$$

We set

$$\mathbf{S}_1 = \mathbf{V_P} \mathbf{\Sigma_P}^{-\frac{1}{2}} \mathbf{V_P}^T. \tag{C3}$$

Note that $\mathbf{\Sigma_P}^{-\frac{1}{2}}$ exists *only if* $\mathbf{P}$ *is positive definite* (ie., every diagonal elements of $\mathbf{\Sigma_P}$ are positive).

We set $\mathbf{S}_2$ to be the transpose of the eigenvector matrix of $\mathbf{Y} = \mathbf{S}_1 \mathbf{Q} \mathbf{S}_1^T$ (ie, $\mathbf{S}_2 = \mathbf{V}_\mathbf{Y}^T$ where $[\mathbf{V_Y}, \mathbf{\Sigma_Y}] = eig(\mathbf{Y})$).

Then the following relationship will hold

$$\mathbf{S}_2 \mathbf{Y} \mathbf{S}_2^T = \mathbf{\Sigma_Y}. \tag{C4}$$

Note that eigenvector matrices are always orthogonal therefore

$$\mathbf{V_P} \mathbf{V_P}^T = \mathbf{V_P}^T \mathbf{V_P} = \mathbf{S}_2 \mathbf{S}_2^T = \mathbf{S}_2^T \mathbf{S}_2 = \mathbf{I}_{4\times 4} \tag{C5}$$

Firstly, we need to prove that $\mathbf{S P S}^T = \mathbf{I}_{4\times 4}$

$$\begin{aligned}
\mathbf{S P S}^T &= \mathbf{S}_2 \mathbf{S}_1 \mathbf{P} \mathbf{S}_1^T \mathbf{S}_2^T \\
&= \mathbf{S}_2 (\mathbf{V_P} \mathbf{\Sigma_P}^{-\frac{1}{2}} \mathbf{V_P}^T)(\mathbf{V_P} \mathbf{\Sigma_P} \mathbf{V_P}^T)(\mathbf{V_P} \mathbf{\Sigma_P}^{-\frac{1}{2}} \mathbf{V_P}^T) \mathbf{S}_2^T \\
&= \mathbf{S}_2 \mathbf{\Sigma_P}^{-\frac{1}{2}} \mathbf{\Sigma_P} \mathbf{\Sigma_P}^{-\frac{1}{2}} \mathbf{S}_2^T \quad \text{(due to (C5))} \\
&= \mathbf{S}_2 \mathbf{S}_2^T \\
&= \mathbf{I}_{4\times 4} \quad \text{(due to (C5))}
\end{aligned}$$

Secondly, we need to prove $\mathbf{S Q S}^T = \mathbf{Q}_D$ where $\mathbf{Q}_D$ is diagonal.

$$\begin{aligned}
\mathbf{S Q S}^T &= \mathbf{S}_2 \mathbf{S}_1 \mathbf{Q} \mathbf{S}_1^T \mathbf{S}_2^T \\
&= \mathbf{S}_2 \mathbf{Y} \mathbf{S}_2^T \\
&= \mathbf{\Sigma_Y} \quad \text{(diagonal matrix of eigenvalues)}
\end{aligned}$$

THIS PAGE HAS BEEN
INTENTIONALLY LEFT BLANK

Appendix D: Lagrange Multiplier Boundary

We need to show that the optimal Lagrange multiplier must be upper bounded by $\frac{1}{\mu_1}$. From Section 3.4, the Langrangian of the problem is

$$L(\mathbf{y},\lambda) = \mathbf{y}^T\mathbf{y} + 2\mathbf{g}^T\mathbf{y} + u - \lambda(\mathbf{y}^T\mathbf{Q}_D\mathbf{y} - 1) \tag{D1}$$

The first order optimality condition was

$$\frac{\partial L}{\partial \mathbf{y}} = 2(\mathbf{y} + \mathbf{g} - \lambda^*\mathbf{Q}_D\mathbf{y}) = 2((\mathbf{I} - \lambda^*\mathbf{Q}_D)\mathbf{y} + \mathbf{g}) = \mathbf{0}. \tag{D2}$$

The second order optimality condition is

$$\frac{\partial^2 L}{\partial \mathbf{y}^2} = (\mathbf{I} - \lambda^*\mathbf{Q}_D) \geq \mathbf{0} \tag{D3}$$

$$\mathbf{I} - \lambda^*\mathbf{Q}_D = \begin{bmatrix} 1-\lambda^*\mu_1 & 0 & 0 & 0 \\ 0 & 1-\lambda^*\mu_2 & 0 & 0 \\ 0 & 0 & 1 & 0 \\ 0 & 0 & 0 & 1 \end{bmatrix} \geq \mathbf{0}_{4\times 4} \text{ where } \mu_1 > \mu_2 \tag{D4}$$

From (D4), λ^* must satisfy both $\lambda^* \leq 1/\mu_1$ and $\lambda^* \leq 1/\mu_2$. Since $\mu_1 > \mu_2$, by taking the intersection of the two boundary conditions, we arrive at this condition.

$$\lambda^* \leq 1/\mu_1 \tag{D5}$$

DEFENCE SCIENCE AND TECHNOLOGY ORGANISATION DOCUMENT CONTROL DATA	1. PRIVACY MARKING/CAVEAT (OF DOCUMENT)

2. TITLE	3. SECURITY CLASSIFICATION (FOR UNCLASSIFIED REPORTS THAT ARE LIMITED RELEASE USE (L) NEXT TO DOCUMENT CLASSIFICATION)
Landmark-based Navigation of an Unmanned Ground Vehicle (UGV)	Document (U) Title (U) Abstract (U)
4. AUTHOR(S) Jijoong Kim and Hatem Hmam	5. CORPORATE AUTHOR DSTO Defence Science and Technology Organisation PO Box 1500 Edinburgh South Australia 5111 Australia

6a. DSTO NUMBER	6b. AR NUMBER	6c. TYPE OF REPORT	7. DOCUMENT DATE
DSTO-TR-2260	AR-014-415	Technical Report	March 2009

8. FILE NUMBER	9. TASK NUMBER	10. TASK SPONSOR	11. NO. OF PAGES	12. NO. OF REFERENCES
2008/1126788	07/249	CWSD	37	8

13. URL on the World Wide Web	14. RELEASE AUTHORITY
http://www.dsto.defence.gov.au/corporate/reports/DSTO-TR-2260.pdf	Chief, Weapons Systems Division

15. SECONDARY RELEASE STATEMENT OF THIS DOCUMENT

Approved for public release

OVERSEAS ENQUIRIES OUTSIDE STATED LIMITATIONS SHOULD BE REFERRED THROUGH DOCUMENT EXCHANGE, PO BOX 1500, EDINBURGH, SA 5111

16. DELIBERATE ANNOUNCEMENT

No Limitations

17. CITATION IN OTHER DOCUMENTS Yes

18. DSTO RESEARCH LIBRARY THESAURUS http://web-vic.dsto.defence.gov.au/workareas/library/resources/dsto_thesaurus.shtml

Landmark, Navigation, Optimisation

19. ABSTRACT

We present a method for estimating the position and orientation of a ground vehicle in an environment with landmarks. From the geometric relationships, we derive a set of linear equations with a quadratic constraint, which forms the basis for our optimisation problem. We also extend the problem to associating two sets of measurements taken at two successive locations to improve the navigation accuracy. This method is efficient and the performance is robust against large measurement errors.